DOI: 10.1002/ejic.200900921

Dihydroxy- and Tetrahydroxydicarbahemiporphyrazine: Phthalocyanine Analogues with Phenol and Resorcinol Units

Natalie Barone,[a] Roshinee Costa,[a] Saovalak Sripothangnok,[a] and Christopher J. Ziegler*[a]

Keywords: Hemiporphyrazines / Phthalocyanines / Silver / Carbahemiporphyrazines / Agostic interactions

The synthesis of the phthalocyanine variant dicarbahemiporphyrazine (**1**) follows a simple Schiff base condensation protocol, and can be readily modified to incorporate a variety of modified benzene rings into the macrocycle. In this report, we present the synthesis of dihydroxydicarbahemiporphyrazine (**2**) and tetrahydroxydicarbahemiporphyrazine (**3**), hemiporphyrazines in which two phenol and two resorcinol groups, respectively, have been incorporated into the backbone of the macrocycle. The structures of the two macrocycles have been elucidated by X-ray diffraction, and both adopt planar conformations due to the tautomerization of the internal hydrogen atoms to *meso* nitrogen positions. The Ag^{I} complexes of both rings are also presented, and the structures of both complexes Ag**2** and Ag**3** have also been elucidated by single-crystal X-ray methods. In both Ag**2** and Ag**3**, the structures of the macrocycles closely resemble that observed in the Ag^{I} complex of **1**, where the metal atom adopts a three-coordinate geometry with two agostic-type interactions with the internal C–H units from the phenol or resorcinol rings.

Introduction

Since the 1990s, the model chemistry of the heme macrocycle has expanded significantly to include modified porphyrin structures.[1] The backbone of porphyrin can be altered in a number of ways to afford new metal-binding macrocycles. For example, the porphine ring can be isomerized either through skeletal rearrangement, as seen in porphycene,[2] or by inversion of a pyrrole, as observed in N-confused porphyrin.[3] Alternatively, the ring can be modified by expansion, contraction, or modification at the core or at the periphery of the macrocycle. These isomers and analogues of porphyrin have found use as model complexes due to their ability to stabilize oxidation states and electronic configurations similar to those found in enzymatic intermediates.[4] Alternatively, modifications to the porphyrin skeleton can provide insight into the biological selection of porphyrin.[5]

Although investigations into the metal chemistry of the porphyrinoids has been very active over the past two decades, less work has been carried out on azaporphyrin or phthalocyanine analogues and isomers. One important class of phthalocyanine analogue was developed more than five decades ago, first by Linstead and followed by Elvidge.[6] These macrocycles, where one or two of the diiminoisoindoline units are replaced with other rings, are collectively known as the hemiporphyrazines, based on a nomenclature coined by Campbell.[7] In spite of the age of the hemiporphyrazines, surprisingly little metal chemistry has been carried out on these macrocycles.[8]

In our laboratory, we have been investigating the chemistry of hemiporphyrazines that have carbon atoms at the metal-binding core, which we refer to as the carbahemiporphyrazines.[9] These macrocycles show broad similarities to the carbaporphyrin family of porphyrinoids, which includes benziporphyrin,[10] azuliporphyrin,[11] and N-confused porphyrin.[3] The introduction of a carbon atom at the core of a porphyrinoid significantly alters the metal-binding chemistry of the macrocycle as well as the electronic structure of the bound metal atom. The metal complexes of these macrocycles can be highly relevant to intermediates found in heme proteins, due to their unusual spin states and oxygen activation chemistry.[12] However, in spite of the similarities between the carbahemiporphyrazines and the carbaporphyrins, hemiporphyrazine macrocycles typically are non-aromatic in nature, which can limit their usefulness as heme model complexes.[13] A similar lack of aromaticity has been observed in several carbaporphyrins, such as the benziporphyrins. However, aromaticity in the benziporphyrins can be induced by oxidizing or reducing the ring, which can be facilitated by substitution on the benzene ring to generate a redox-active unit within the porphyrinoid. Specifically, 2-hydroxybenziporphyrin was found to exist as the keto form oxibenziporphyrin.[10,14]

In this report, we present two functionalized versions of dicarbahemiporphyrazine (**1**), where we have introduced the redox-active rings phenol and resorcinol into the backbone

[a] Department of Chemistry, University of Akron, Akron, OH 44325-3601, USA
Fax: +1-330-972-6085
E-mail: ziegler@uakron.edu

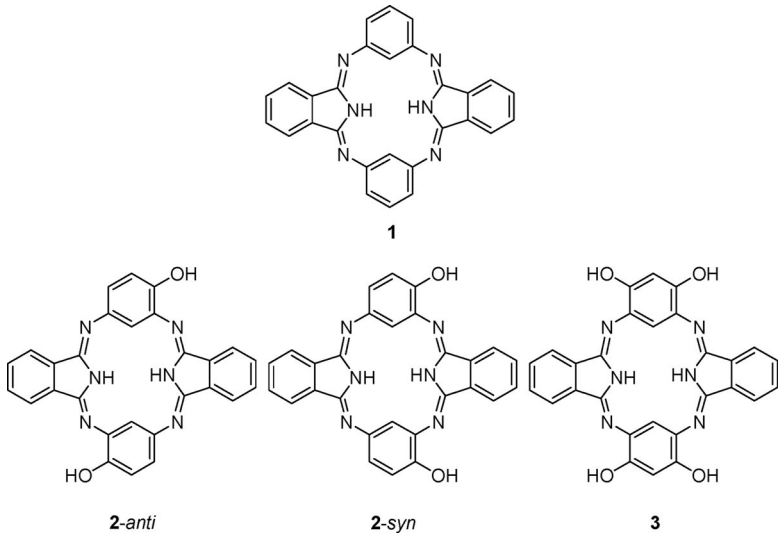

Scheme 1.

of the macrocycle. We have generated these two modified phthalocyanines by replacing the benzene ring in the macrocycle. The structures of these rings are shown in Scheme 1, and we refer to these rings as dihydroxydicarbahemiporphyrazine (**2**) and tetrahydroxydicarbahemiporphyrazine (**3**). Both macrocycles can be generated in good yield, although macrocycle **2** is isolated as two isomers: *syn* and *anti*. Compounds **2** and **3** exhibit a different tautomerization from that seen in unmodified dicarbahemiporphyrazine, and adopt planar structures. In addition, the two macrocycles can also be metalated with silver ions to afford Ag^{I} adducts, which both closely resemble the silver complex of **1**.

Results and Discussion

The incorporation of phenol and resorcinol groups into the backbone of phthalocyanine can be readily accomplished by use of the corresponding *m*-phenylenediamines, diaminophenol and diaminoresorcinol. These can be condensed with diiminoisoindoline by using a modification of Linstead's procedure, shown in Scheme 2. Both diaminophenol and diaminoresorcinol are commercially available as the hydrochloric acid salts, and it has been shown that the hemiporphyrazines are sensitive to acid-catalyzed decomposition.[8] To facilitate the reaction and to prevent loss of the resultant product, triethylamine was added to the

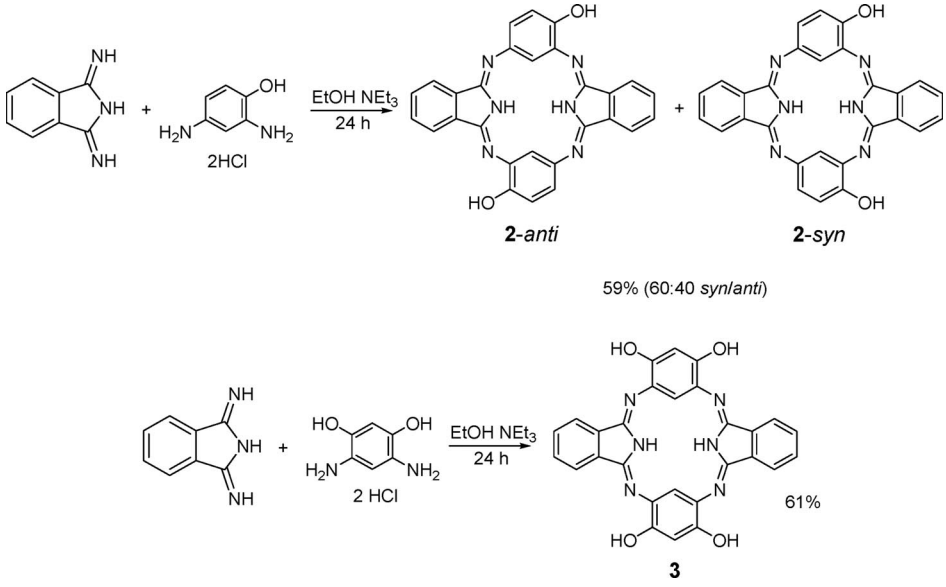

Scheme 2.

reaction solutions. The product yields were generally good, but slightly less than that reported for **1**. The reduction in yield results from the increased solubility of **2** and **3**; similar decreases in yields have also been observed with other hemiporphyrazine macrocycles.[8]

The synthesis of **2** results in two isomers: *syn* and *anti* configurations. We were not able to separate these two isomers by either recrystallization methodologies or chromatography, but we were able to determine the relative ratio of the two products by ^{1}H NMR spectroscopy and observed a 60:40 ratio of the *syn*/*anti* conformers. We were able to grow crystals of the *anti* isomer (which were mixed with amorphous *syn* isomer) and elucidate its structure, shown in Figure 1. Overall, the structure of the complex resembles that of the unmodified dicarbahemiporphyrazine with regard to bond lengths, but the planarity of **2** differs significantly from that seen in the various neutral crystal forms of **1**. Structurally, the *anti* form of **2** has similarities to the dicationic form of **1** recrystallized from formic acid.[9] In both compounds, the reason for the planarity of the macrocycle results from the migration of the interior ionizable protons to exterior *meso* positions. However, it is unclear if this planarity is retained in solution, as will be discussed below. The presence of a proton on the *meso*-carbon atom does lengthen the Schiff base double bonds from ca. 1.29 Å to ca. 1.35 Å, which implies some delocalization in the N–C–N unit in the diiminoisoindoline ring, as shown in Scheme 3.

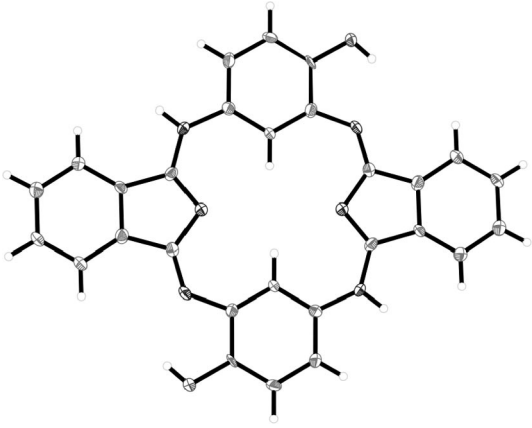

Figure 1. Structure of the *anti* form of **2** with 35% thermal ellipsoids.

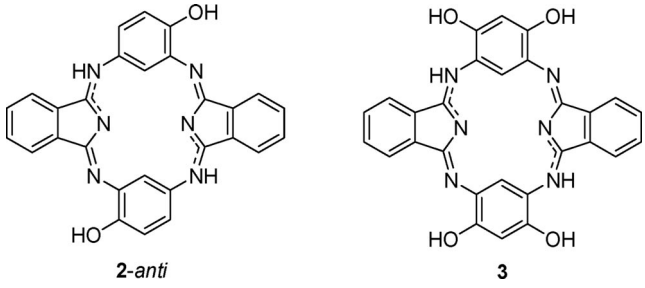

Scheme 3.

The synthesis of compound **3** produces a single isomer, which can be isolated as a pure crystalline solid. Single crystals can be obtained upon recrystallization from pyridine/hexanes. The structure of compound **3** was also elucidated by X-ray crystallography, and it is shown in Figure 2. As in the *anti* form of **2**, compound **3** is rigidly planar, and the bonding in the ring is shown in Scheme 3. Unlike compound **2**, however, **3** may retain its planarity in solution, as will be discussed below. In the free base, we observe hydrogen-bonding interactions between the resorcinol alcohol groups and the *meso*-nitrogen positions. Along with the expected OH–N hydrogen bonds, there are also NH–O hydrogen bonds, and we believe that these interactions help stabilize the external tautomer and thus the planar conformation of the macrocycle. In addition to these intramolecular hydrogen-bonding interactions, there are also hydrogen bonds between the solvent pyridine molecules and the resorcinol ring OH groups. With regard to bond lengths and angles, compound **3** resembles **2**, and has similar Schiff base bond lengths (ca. 1.29 Å and ca. 1.34 Å, respectively, for the deprotonated and protonated C–N double bonds).

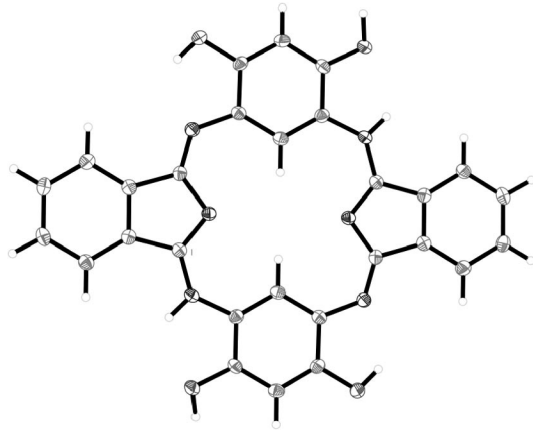

Figure 2. Structure of **3** with 35% thermal ellipsoids.

One of the notable aspects of both macrocycles is that they exhibit absorption spectra that are markedly different from their parent dicarbahemiporphyrazine. Figure 3 displays the spectra of **2**–**3** in DMF. Compound **1** shows no significant absorption features in the visible region, due to the localization of the aromaticity on the benzene and isoindoline rings. Previously, compound **1** has been shown to be non-planar, which prevents significant overlap between rings in the macrocycle.[9] Macrocycle **2** shows a high energy absorption at 376 nm and a shoulder at approximately 430 nm, with the peak exhibiting an extinction coefficient of 1.10×10^4 M^{-1} cm^{-1}. It is important to note that because **2** is a mixture, we cannot specifically assign these features to either the *syn* or *anti* isomer. In contrast to both **1** and **2**, compound **3** shows very intense absorptions above 650 nm extending into the near IR. We observe peaks at 672, 701 and 725 nm, and the extinction coefficients for these peaks are 1.70×10^4, 1.84×10^4 and 1.98×10^4 M^{-1} cm^{-1}. It is important to note that the X-ray-elucidated structures of both **2** and **3** reveal the macrocycles to have localized aromaticity

on the phenyl and isoindoline units, and there are no observable ring current effects in the ^{1}H NMR spectra. Thus, we believe that the absorptions result from intramolecular charge-transfer transitions, rather than from a π-to-π* transition as seen in porphyrins and phthalocyanines. The planarity of the macrocycles may affect this transition; we speculate that compound **3** may be planar in solution, whereas **2** may have a saddle shape as seen in **1**. However, in spite of the fundamental difference in the nature of the transitions, these absorptions can still be used to probe the electronic structures of these rings.

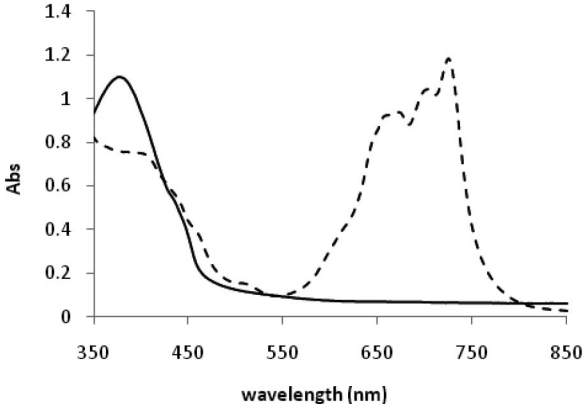

Figure 3. UV/Vis spectra of **2** (solid line) and **3** (dashed line) in DMF.

We have begun to investigate the metalation chemistry of compounds **2** and **3**, and in our initial foray into this chemistry we have isolated the silver(I) complexes for both macrocycles. Ag**2** and Ag**3** can be prepared by reaction of $AgNO_3$ with the free-base macrocycles in pyridine solution. The products are isolated as the nitrate salts; the macrocycles are protonated at two of the external nitrogen *meso* positions, resulting in a monocationic charge for both Ag**2** and Ag**3**. Figure 4 shows thermal ellipsoid diagrams of the disordered structure of Ag**2** and the non-disordered Ag**3**. Since compound **2** appears as two isomers, the resultant silver adduct also appears as the *syn* and *anti* isomers. X-ray structural elucidation of a crystal from the reaction mixture revealed that the *syn* and *anti* isomers co-crystallize, resulting in the two orientations of the oxygen atom shown in the figure. The hydroxy groups on one of the two benzene rings are disordered with a 60:40 *syn*/*anti* ratio, identical to that observed in the ^{1}H NMR spectrum of **2**.

The structures of both Ag**2** and Ag**3** closely resemble the silver adduct of **1**, which we presented in an earlier communication.[9] The metal atoms are essentially three-coordinate, with Ag–N bonds to the two diiminoisoindoline nitrogen atoms in the macrocycle and one nitrogen atom from an axial pyridine ligand. The macrocycle itself adopts a saddle-type conformation, with the two isoindoline rings tilted up toward the metal ion, whereas the phenol and resorcinol rings are tilted away from the metal centre. The Ag–N bond lengths are 2.331(4) Å and 2.383(4) Å in Ag**2** and 2.361(3) Å and 2.364(3) Å in Ag**3**. The axial Ag–N bonds are slightly shorter, with identical distances observed in Ag**2**

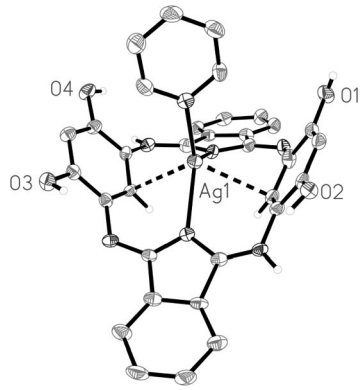

Figure 4. Structures of Ag**2** (left) and Ag**3** (right) with 35% thermal ellipsoids. All hydrogen atoms, solvent and nitrate anions have been omitted for clarity, with the exception of those on the internal carbon positions, the hydroxy groups and the externally protonated *meso*-nitrogen positions. In Ag**2**, the oxygen positions O2 and O3 are disordered with 60:40 occupancy, corresponding to the *syn*/*anti* isomers. In Ag**3**, the nitrate anion is omitted for clarity.

[2.255(4) Å] and Ag**3** [2.260(4) Å]. The phenol and resorcinol rings of Ag**2** and Ag**3** form agostic-type bonds with the silver ions, similar to those seen in the Li, Mn, Fe, and Co adducts of **1**. The Ag–C bond lengths are in the range of 2.66–2.67 Å, identical to those seen in the silver complex of **1**.

The change in structures from planar to saddle-shaped upon metallation with silver ions does raise the question of the effect on the UV/Vis spectra. We speculated above that the absorptions observed in **3** may arise from a planar structure present in the solution phase; this can be readily tested by investigating the spectra of Ag**3**, where the macrocycle clearly deviates from planarity. Figure 5 shows the spectra of Ag**2** and Ag**3** in DMF. The spectrum of Ag**2** resembles that seen for **2**; however, for Ag**3**, we note marked differences from the spectrum of **3**. Transitions are still observed above 650 nm, but the extinction coefficients for these bands are appreciably reduced vs. the free base. The maximum occurs at 729 nm, with $\varepsilon = 3.35 \times 10^3$ M^{-1} cm^{-1}.

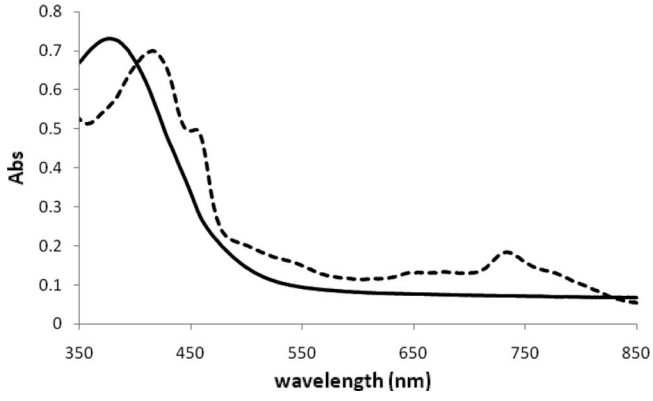

Figure 5. UV/Vis spectra of Ag**2** (solid line) and Ag**3** (dashed line) in DMF.

This decrease is consistent with a change in planarity of the hemiporphyrazine, and we are continuing our investigations into the UV/Vis transitions in these macrocycles.

Conclusions

We report the incorporation of phenol and resorcinol rings into the backbone of the dicarbahemporphyrazine macrocycle. Dihydroxy- and tetrahydroxydicarbahemiporphyrazines can be generated in good yield by means of a Schiff base condensation reaction between diaminophenol and diaminoresorcinol, respectively, in the presence of base. The resultant rings are planar, in contrast to most of the structures of the unmodified parent ring. Silver can be readily inserted into both **2** and **3**, and the resultant complexes show low-coordinate metal sites with agostic-type bonding interactions. We are continuing this work on these macrocycles and investigating their redox behavior.

Experimental Section

General Methods: All reagents and solvents were purchased from Sigma, Aldrich or Acros Organics and were used without further purification. Mass spectra were recorded by using an LCT electrospray spectrophotometer at the Mass Spectrometry and Proteomics Facility of Ohio State University. Elemental analyses were conducted at the University of Illinois, School of Chemical Sciences Microanalysis Laboratory. ^{1}H and ^{13}C NMR spectroscopic data were collected with a Varian Mercury 300 MHz NMR spectroscopy. Additional ^{1}H COSY data were collected with a Varian INOVA 750 MHz NMR spectrometer at The University of Akron. Single-crystal X-ray intensity data were measured at 100 K (Bruker KYRO-FLEX) with a Bruker SMART APEX CCD-based X-ray diffractometer system equipped with an Mo-target X-ray tube (λ = 0.71073 Å) operated at 2000 W power. The crystals were mounted on a cryoloop by using Paratone N-Exxon oil and placed under a stream of nitrogen at 100 K. The detector was placed at a distance of 5.009 cm from the crystals. The data were corrected for absorption with the SADABS program.[15] The structures were refined by using the Bruker SHELXTL Software Package (Version 6.1),[15] and were solved by direct methods until the final anisotropic full-matrix, least-squares refinement of F^2 converged. Additional experimental details are provided in Table 1. CCDC-747403 (for **2**-*anti*), -747404 (for **3**), -747405 (for Ag**2**), -747406 (for Ag**3**) contain the supplementary crystallographic data for this paper. These data can be obtained free of charge from The Cambridge Crystallographic Data Centre via www.ccdc.cam.ac.uk/data_request/cif.

Preparation of *syn*/*anti*-Dihydroxydicarbahemiporphyrazine (2): The macrocycle was prepared by using a slight modification of the procedure described in the literature for hemiporphyrazine. Diiminoisoindoline (2.00 g, 13.8 mmol) and diaminophenol dihydrochloride (2.71 g, 13.8 mmol) were heated together in ethanol (25 mL) and triethylamine (2 mL) in the dark for 24 h. The initial reaction mixture changed to a brownish-red color, followed by the formation of a yellow precipitate. The reaction mixture was then filtered, and the yellow precipitate was collected, washed with ethanol and dried in air. Yield of *syn*/*anti* isomer mixture: 2.43 g (59%). Single crystals of the *anti* isomer that were suitable for X-ray structural elucidation were grown from the product mixture by using DMF. ^{1}H NMR ([D$_6$]DMSO, 300 MHz): δ = 10.83 (d, 2 H, OH), 10.50 (s, 1 H, OH), 10.30 (s, 1 H, OH), 10.22 (d, 2 H, OH), 8.26 (d, 2 H, NH), 8.17 (d, 2 H, NH), 7.92 (m, 4 H, Ph), 7.80 (m, 4 H, Ph), 7.58 (t, 2 H, Ph), 7.16 (d, 2 H, Ph), 6.91 (d, 2 H, Ph) ppm. ^{13}C NMR ([D$_6$]DMSO, 300 MHz): δ = 149.2, 133.1, 132.3, 131.7, 122.9, 122.3, 117.4, 48.62 ppm. ESI MS (positive ion): calcd. for [**1**]$^+$ 470.52; found 470.1. $C_{28}H_{18}N_6O$ (454.48): calcd. C 71.48, H 3.86, N 17.86; found C 70.87, H 4.04, N 17.66. Crystal data and structure refinement are summarized in Table 1.

Preparation of Tetrahydroxydicarbahemiporphyrazine (3): The macrocycle was prepared according to the same general methodology as **2**. Diiminoisoindoline (1.45 g, 10.0 mmol) was dissolved in hot ethanol (15 mL). Diaminoresorcinol dihydrochloride (2.05 g, 10.0 mmol) and triethylamine (2 mL) were added to the solution. The reaction mixture was then brought to reflux in the dark for

Table 1. X-ray data collection and structure parameters for **2**-*anti*, **3**, Ag**2** and Ag**3**.

	2-*anti*	**3**	Ag**2**	Ag**3**
Empirical formula	$C_{34}H_{32}N_8O_4$	$C_{42}H_{32}N_{10}O_4$	$AgC_{38}H_{25}N_7O_2$	$AgC_{48}H_{39}N_{11}O_7$
Formula mass	616.68	740.78	735.55	989.76
Crystal system	triclinic	triclinic	monoclinic	orthorhombic
Space group	$P\bar{1}$	$P\bar{1}$	$P2_1/n$	$Pbca$
a [Å]	7.670(3)	6.2831(11)	13.806(3)	18.434(3)
b [Å]	9.449(3)	11.1829(19)	18.134(4)	20.511(3)
c [Å]	11.205(4)	12.702(2)	17.280(3)	30.663(5)
α [°]	105.199(6)	85.382(3)	90	90
β [°]	99.703(7)	81.490(3)	112.930(4)	90
γ [°]	101.402(7)	77.458(3)	90	90
Volume [Å^3]	747.1(5)	860.5(3)	3984.3(13)	11594(3)
Z	1	1	4	8
$\rho_{calcd.}$ [Mg/m^3]	1.371	1.429	1.528	1.133
μ [mm^{-1}]	0.093	0.096	0.570	0.399
F(000)	324	386	1872	4048
Reflections collected	2468	3653	32850	93807
Independent reflections	1537 [R(int) = 0.0967]	2996 [R(int) = 0.0215]	8642 [R(int) = 0.0965]	12663 [R(int) = 0.1517]
GOF on F^2	1.064	1.036	1.023	0.636
$R[I>2\sigma(I)]$	R_1 = 0.0810, wR_2 = 0.1919	R_1 = 0.0448, wR_2 = 0.1146	R_1 = 0.0714, wR_2 = 0.1656	R_1 = 0.0639, wR_2 = 0.1869
R(all data)	R_1 = 0.1291, wR_2 = 0.2181	R_1 = 0.0556, wR_2 = 0.1203	R_1 = 0.1268, wR_2 = 0.1850	R_1 = 0.1170, wR_2 = 0.2135

24 h. The solution was initially black in color and did not change over the course of the reaction. The reaction mixture was then filtered, and the black-red precipitate was collected, recrystallized from DMF/ethanol and dried in air. Yield 2.97g (61%). Single crystals of **3** that were suitable for X-ray structural elucidation were grown from pyridine/hexanes. ^{1}H NMR ([D$_6$]DMSO, 300 MHz): δ = 11.2 (s, 2 H, OH), 10.55 (s, 2 H, OH), 8.19 (s, 2 H, NH), 7.96 (m, 4 H, Ph), 7.54 (m, 4 H, Ph), 6.42 (s, 2 H, Ph), 5.61 (s 2 H, Ph) ppm. ^{13}C NMR ([D$_6$]DMSO, 300 MHz): δ = 172.7, 134.9, 131.3, 123.0, 122.2, 103.3, 98.1, 45.5 ppm. ESI MS (positive ion): calcd. for [**3**]$^+$: 502.48; found 503.1 [M + H]. $C_{33}H_{31}N_7O_7$ (**3**·DMF·EtOH·H_2O, 637.64): calcd. C 62.16, H 4.90, N 15.38; found C 62.36, H 4.59, N 15.89. Crystal data and structure refinement are summarized in Table 1.

Ag2: The Ag^I complex was prepared from **2** (282 mg, 0.6 mmol) dissolved in pyridine (10 mL). $AgNO_3$ (102 mg, 0.6 mmol) was slowly added to the solution with stirring in air at room temperature. The mixture was stirred at room temperature for 30 min. The resulting dark red solution was filtered, and the filtrate was layered with diethyl ether. Red crystals of Ag**2** were collected after 3 d. Yield: 0.014 g (40.4%). ^{1}H NMR ([D$_6$]DMSO, 300 MHz): δ = 11.35 (s, 2 H, OH), 8.34 (d, 2 H, NH), 7.83 (t, 2 H, Ph), 7.65 (m, 4 H, Ph), 7.56 (m, 4 H, Ph), 7.26 (s, 2 H, Ph), 7.09 (s, 2 H, Ph), 6.12 (s, 2 H, Ph) ppm. ^{13}C NMR ([D$_6$]DMSO, 300 MHz): δ = 148.1, 138.5, 134.4, 130.8, 128.4, 126.8, 124.2, 123.0 ppm. HR ESI MS (positive ion): calcd. for [Ag**2** – py – NO_3^-]$^+$: 577.3; found 577.0. $C_{33}H_{23}Ag_1N_8O_5$ (719.45): calcd. C 55.09, H 3.22, N 15.78; found C 55.71, H 3.45, N 14.91. Crystal data and structure refinement are summarized in Table 1.

Ag3: Compound **3** (0.301 g, 0.6 mmol) was dissolved in pyridine (10 mL). $AgNO_3$ (0.103 g, 0.6 mmol) was slowly added to the above solution with stirring. The reaction mixture was stirred at room temperature for 30 min, after which there was no precipitate present. The solution was then layered with hexanes. Dark, reddish black crystals were observable after 3 d. The crystals appeared to be light-sensitive and were handled under darkness. Yield 0.14 g (38.3%). ^{1}H NMR ([D$_6$]DMSO, 300 MHz): δ = 11.31 (s, 4 H, OH), 8.64 (s, 2 H, NH), 7.83 (m, 4 H, Ph), 7.52 (m, 4 H, Ph), 7.09 (s, 2 H, Ph), 6.92 (s, 2 H, Ph) ppm. ^{13}C NMR ([D$_6$]DMSO, 300 MHz): δ = 150.3, 149.9, 136.9, 136.2, 131.4, 124.3, 121.9, 104.2 ppm. HR ESI MS (positive ion): calcd. for [Ag**3** – py – NO_3^-]$^+$ 610.3; found 609.0. $C_{38}H_{28}Ag_1N_9O_7$ (Ag**3**·py, 830.55): calcd. C 54.95, H 3.40, N 15.18; found C 54.01, H 3.42, N 14.59. Crystal data and structure refinement are summarized in Table 1.

Acknowledgments

We wish to acknowledge the National Science Foundation (Grant CHE-0616416) for funds used in this research.

[1] a) J. L. Sessler, S. J. Weghorn, *Expanded, Contracted, and Isomeric Porphyrins*, Pergamon, New York, **1997**; b) K. M. Kadish, K. M. Smith, R. Guilard, *The Porphyrin Handbook*, Academic Press, New York, **2000**, vol. 1–2; c) A. Ghosh, *Angew. Chem. Int. Ed.* **2004**, *43*, 1918–1931; d) J. D. Harvey, C. J. Ziegler, *J. Inorg. Biochem.* **2006**, *100*, 869–880.

[2] a) C. J. Fowler, J. L. Sessler, V. M. Lynch, J. Waluk, A. Gebauer, J. Lex, A. Heger, F. Zuniga-y-Rivero, E. Vogel, *Chem. Eur. J.* **2002**, *8*, 3485–3496; b) D. Sanchez-Garcia, J. L. Sessler, *Chem. Soc. Rev.* **2008**, *37*, 215–232.

[3] a) H. Furuta, T. Asano, T. Ogawa, *J. Am. Chem. Soc.* **1994**, *116*, 767–768; b) P. J. Chmielewski, L. Latos-Grażyński, K. Rachlewicz, T. Glowiak, *Angew. Chem. Int. Ed. Engl.* **1994**, *33*, 779–781; c) G. R. Geier, D. M. Haynes, J. S. Lindsey, *Org. Lett.* **1999**, *1*, 1455–1458.

[4] J. D. Harvey, C. J. Ziegler, *J. Inorg. Biochem.* **2006**, *100*, 869–880.

[5] C. J. Ziegler, in *Advances in Inorganic Biochemistry: From Synthetic Models to Cellular Systems* (Eds.: E. C. Long, M. J. Baldwin), ACS Symposium Series, Washington DC, **2009**, vol. 1012, pp. 115–132.

[6] a) J. A. Elvidge, R. P. Linstead, *J. Chem. Soc.* **1952**, 5008–5012; b) P. F. Clark, J. A. Elvidge, R. P. Linstead, *J. Chem. Soc.* **1954**, 2490–2497.

[7] J. B. Campbell, U. S. Patent 2765308, **1956**; *Chem. Abstr.* **1956**, *51*, 8143f.

[8] F. Fernandez-Lazaro, T. Torres, B. Hauschel, M. Hanack, *Chem. Rev.* **1998**, *98*, 563–575.

[9] a) W. S. Durfee, C. J. Ziegler, *J. Porphyrins Phthalocyanines* **2009**, *13*, 304–311; b) A. Çetin, W. S. Durfee, C. J. Ziegler, *Inorg. Chem.* **2007**, *46*, 6239–6241; c) Q. Wu, A. Çetin, W. S. Durfee, C. J. Ziegler, *Angew. Chem. Int. Ed.* **2006**, *45*, 5670–5673; d) S. Sripothongnak, A. Pischera, M. P. Espe, C. J. Ziegler, *Inorg. Chem.* **2009**, *48*, 1293–1300; e) S. Sripothongnak, N. V. Barone, C. J. Ziegler, *Chem. Commun.* **2009**, 4584–4586.

[10] a) M. Stepien, L. Latos-Grażyński, *Acc. Chem. Res.* **2005**, *38*, 88–98; b) M. Stepien, L. Latos-Grażyński, T. D. Lash, L. Szterenberg, *Inorg. Chem.* **2001**, *40*, 6892–6900; c) M. Stepien, L. Latos-Grażyński, L. Szterenberg, *J. Org. Chem.* **2007**, *72*, 2259–2270.

[11] a) S. R. Graham, D. A. Colby, T. D. Lash, *Angew. Chem. Int. Ed.* **2002**, *41*, 1371–1374; b) T. D. Lash, *Chem. Commun.* **1998**, 1683–1684.

[12] W. D. Woggon, *Acc. Chem. Res.* **2005**, *38*, 127–136.

[13] S. Sripothongnak, N. V. Barone, A. Çetin, R. Wu, W. S. Durfee, C. J. Ziegler, *J. Porph. Phthal.*, in press.

[14] a) T. D. Lash, S. T. Chaney, D. T. Richter, *J. Org. Chem.* **1998**, *63*, 9076–9088; b) J. A. El-Beck, T. D. Lash, *Org. Lett.* **2006**, *8*, 5263–5266.

[15] G. M. Sheldrick, *SHELXTL, Crystallographic Software Package*, version 6.10, Bruker-AXS, Madison, WI, **2000**.

Received: September 15, 2009
Published Online: December 18, 2009

